EUROPEAN ORGANIZATION FOR NUCLEAR RESEARCH

First measurement of prompt and non-prompt D^{*+} vector meson spin alignment in pp collisions at $\sqrt{s} = 13$ TeV

ALICE Collaboration

Abstract

This letter reports the first measurement of spin alignment, with respect to the helicity axis, for D^{*+} vector mesons and their charge conjugates from charm-quark hadronisation (prompt) and from beauty-meson decays (non-prompt) in hadron collisions. The measurements were performed at midrapidity ($|y| < 0.8$) as a function of transverse momentum (p_T) in proton–proton (pp) collisions collected by ALICE at the centre-of-mass energy $\sqrt{s} = 13$ TeV. The diagonal spin density matrix element ρ_{00} of D^{*+} mesons was measured from the angular distribution of the $D^{*+} \rightarrow D^0(\rightarrow K^-\pi^+)\pi^+$ decay products, in the D^{*+} rest frame, with respect to the D^{*+} momentum direction in the pp centre of mass frame. The ρ_{00} value for prompt D^{*+} mesons is consistent with $1/3$, which implies no spin alignment. However, for non-prompt D^{*+} mesons an evidence of ρ_{00} larger than $1/3$ is found. The measured value of the spin density element is $\rho_{00} = 0.455 \pm 0.022(\text{stat.}) \pm 0.035(\text{syst.})$ in the $5 < p_T < 20$ GeV/c interval, which is consistent with a PYTHIA 8 Monte Carlo simulation coupled with the EVTGEN package, which implements the helicity conservation in the decay of D^{*+} meson from beauty mesons. In non-central heavy-ion collisions, the spin of the D^{*+} mesons may be globally aligned with the direction of the initial angular momentum and magnetic field. Based on the results for pp collisions reported in this letter it is shown that alignment of non-prompt D^{*+} mesons due to the helicity conservation coupled to the collective anisotropic expansion may mimic the signal of global spin alignment in heavy-ion collisions.

1 Introduction

The production of hadrons containing heavy quarks, i.e. charm and beauty, has been extensively studied in both lepton and hadron collisions, improving significantly the understanding of the hadronisation mechanism [1–8]. However, several aspects of the transition of the heavy quark to the final-state hadron are not yet settled. One of them regards the spin properties of produced particles in the quark hadronisation. In the limit of very large heavy-quark mass ($m_Q \rightarrow \infty$), the polarisation of heavy-flavour baryons is assumed to be that carried by the heavy valence quark [9]. This assumption was studied at LEP in e$^+$e$^-$ collisions where the polarisation of Λ_b^0 baryons was used to probe the electroweak structure of the Z^0 boson production and decays [10–14]. In hadronic collisions, the polarisation of Λ_b^0 baryons can arise during the hadronisation process if beauty quarks are produced with a transverse polarisation, as predicted by the heavy-quark effective theory [9, 11]. At this time, one measurement, performed by the LHCb Collaboration, found no significant polarisation [15]. For vector mesons with quantum numbers $J^P = 1^-$, both in lepton and hadron collisions, at least part of the polarisation should arise from the hadronisation process [9]. Models based on statistical quantum mechanics considerations [16, 17], heavy-quark effective theory [9], or inspired by quantum chromodynamics (QCD) [18] provide very different predictions, from no polarisation, to very large longitudinal or transverse polarisation. This aspect of the hadronisation is typically not accounted for in QCD-inspired Monte Carlo (MC) generators based on the Lund string model [19], such as PYTHIA 8 [20, 21], or the clustering model [22], as implemented in HERWIG 7 [23]. Measurements of excited B vector meson states in Z^0 decays at LEP did not show any significant polarisation [24, 25]. For charm vector mesons (D^{*+}) a longitudinal polarisation was observed by OPAL [26]. However, previous measurements in e$^+$e$^-$ collisions indicated no significant polarisation for D^{*+} mesons [27–29].

The polarisation of vector mesons containing heavy quarks in heavy-ion collisions is of special interest. The initial stages of such collisions, with non-zero impact parameter, are expected to be characterised by a large orbital angular momentum [30] and a strong magnetic field [31–33]. These initial conditions could influence the produced colour-deconfined matter (called quark–gluon plasma [34]). The directions of the angular momentum and the magnetic field in such collisions are perpendicular to the reaction plane (subtended by the beam axis and impact parameter) [35]. Theoretical calculations at LHC energies predict the values of the angular momentum to be of the order of 10^7 $\hbar$ [30] and the magnetic field to be about 10^{16} T [31–33, 36, 37]. While the angular momentum, a conserved quantity in strong interactions, is expected to affect the whole evolution of the collision, the magnetic field is transient in nature and its strength falls steeply with time. Heavy quarks are produced at the initial stages of heavy-ion collisions, in a time scale shorter than the quark–gluon plasma formation time [38] and are sensitive to the large initial magnetic field as well as the angular momentum. In the presence of these initial conditions, charm quarks can be polarised. The quark polarisation is expected to be further transferred to the final-state hadrons during hadronisation and it is predicted to be different in the case of hadronisation in vacuum, or recombination with light quarks from the deconfined medium [35, 39–41]. Measurements in heavy-ion collisions indicate that the recombination mechanism is important to describe the production and angular anisotropies of charm hadrons [42–50]. If observed, a non-zero polarisation of D^{*+} mesons will be a manifestation of the angular momentum and the magnetic field created in heavy-ion collisions. The study of D^{*+} mesons would provide additional information, crucial for the interpretation of the recently measured J/ψ polarisation in Pb–Pb collisions by the ALICE Collaboration [51]. In fact, the polarisation of D^{*+} and J/ψ mesons have different contributions from the angular momentum and the magnetic field, given the valence light quark present in the D^{*+} meson, which is expected to be less sensitive than the charm quark to the magnetic field. However, the interpretation of experimental data for heavy-ion collisions requires a baseline study in elementary proton–proton (pp) collisions, where such initial conditions are not expected to form. Moreover, in this study, one of the major source of background is the feed-down contribution of D^{*+} mesons originating from decays of scalar mesons containing a beauty quark, which are observed to be longitudinally polarised by the Belle and LHCb Collaborations

in e$^+$e$^-$ and pp collisions, respectively [52, 53]. This is a direct consequence of the helicity conservation and the Vector–Axial (V−A) nature of the weak interaction involved in the b $\rightarrow$ c decay, which leads to left-handed fermion couplings in interactions with W bosons [54, 55]. It is therefore important to separate contributions to the polarisation from promptly produced mesons and from those originating in beauty-hadron decays.

The polarisation of D^{*+} vector mesons cannot be probed directly as D^{*+} mesons are measured through the parity conserving strong decay D$^{*+} \rightarrow$ D$^0(\rightarrow$ K$^-\pi^+)\pi^+$. However, experimentally, the spin alignment along the quantisation direction can be studied by measuring the diagonal spin density matrix element (ρ_{00}) of the vector meson. The ρ_{00} reflects the probability of finding a vector meson in the state with spin zero out of possible states with spin projection -1, 0, and 1 [56]. If the spin of particles is homogeneously distributed, all spin states are expected to be equally probable, thereby yielding $\rho_{00} = 1/3$. The spin alignment is studied by measuring the angular distribution of the decay products of vector mesons. Their decay products are measured with respect to a quantisation axis, which is the vector meson momentum direction (helicity axis) in pp collisions and the perpendicular direction of the reaction plane in heavy-ion collisions. In the latter, these two axes are further correlated through the anisotropic collective expansion which is quantified by coefficients in a Fourier decomposition of the azimuthal-angle distribution of final-state particle momenta, with the second-harmonic coefficient v_2, called elliptic flow [57], being the dominant one [49]. The angular distribution of the D^{*+} decay products is expressed as

$$\frac{\mathrm{d}N}{\mathrm{d}\cos\theta^*} \propto [1 - \rho_{00} + (3\rho_{00} - 1)\cos^2\theta^*], \tag{1}$$

where θ^* is the angle between the momentum of either the D^0 meson or the pion in the rest frame of the vector meson with respect to the quantisation axis [58].

In this letter, the first measurement of the spin alignment of D^{*+} mesons from charm-quark hadronisation (prompt) and from beauty-hadron decays (non-prompt) at midrapidity is presented as a function of transverse momentum (p_{T}) in pp collisions at a centre-of-mass energy of $\sqrt{s} = 13$ TeV. Based on these measurements, quantitative predictions for the spin distributions of non-prompt D^{*+} meson for a future measurement of the D^{*+}-meson spin alignment in heavy-ion collisions are provided.

2 Experimental apparatus and data analysis

The analysis was performed using about 1.8×10^9 minimum-bias and about 10^9 high-multiplicity triggered pp collisions at $\sqrt{s} = 13$ TeV recorded with the ALICE apparatus [59, 60], corresponding to an integrated luminosity of $\mathscr{L}_{\mathrm{int}} \approx 32$ nb^{-1} and $\mathscr{L}_{\mathrm{int}} \approx 7.7$ pb^{-1}, respectively. The minimum-bias trigger required coincident signals in the two V0 detectors, which are two scintillator arrays covering the pseudorapidity intervals $-3.7 < \eta < -1.7$ and $2.8 < \eta < 5.1$ [61]. The high-multiplicity trigger selected the 0.17% highest-multiplicity events out of all inelastic collisions with at least one charged particle in the pseudorapidity range $|\eta| < 1$, relying on the signal amplitudes of the V0 detectors. Events were further selected offline to remove machine-induced backgrounds [59]. They were required to have a reconstructed collision vertex located within ± 10 cm from the centre of the detector along the beam-line direction to maintain a uniform acceptance. Events with multiple reconstructed primary vertices (pileup) were rejected. Primary vertices were reconstructed from track segments measured with the two innermost layers of the Inner Tracking System (ITS), which consists of six cylindrical layers of silicon detectors [62]. The remaining undetected pileup was studied and found to be negligible for this analysis.

The D^{*+} mesons and their charge conjugates were measured at midrapidity ($|y| < 0.8$) via the D$^{*+} \rightarrow$ D$^0(\rightarrow$ K$^-\pi^+)\pi^+$ decay channel, with branching ratio BR $= (2.67 \pm 0.03)\%$ [63]. The measurement of D^{*+} mesons was based on charged-particle tracks reconstructed with the Time Projection Chamber (TPC) [64] and ITS detectors. The D^0 decay candidates were defined combining pairs of tracks with the expected charge combinations. Each track from the decay was required to have $|\eta| < 0.8$,

$p_{\rm T} > 0.3$ GeV/c, at least 70 (out of 159) associated space points in the TPC, and a minimum of two hits in the ITS, with at least one in either of the two innermost layers to ensure a good pointing resolution. The D^{*+}-meson candidates were reconstructed by combining D^0 candidates with low-$p_{\rm T}$ tracks (referred to as soft pions) having $|\eta| < 0.8$, $p_{\rm T} > 50$ MeV/c, and at least two hits in the ITS. The analysis was based on the reconstruction of decay-vertex topologies of D^0 mesons displaced from the interaction vertex. In particular, the proper decay length of prompt D^0 mesons of $c\tau \approx 123$ μm and that of beauty hadrons of $c\tau \approx 500$ μm were exploited to resolve the D^0-meson decay vertices. In order to reduce the large combinatorial background and to separate the contribution of prompt and non-prompt D^{*+} mesons, a multiclass classification algorithm based on Boosted Decision Trees (BDTs) was used [65, 66]. The candidate information used by the BDT algorithm to distinguish among prompt and non-prompt D^{*+} mesons and background candidates was based on i) the distance between the reconstructed D^0-meson decay vertex and the primary vertex, ii) the D^0-meson and soft-pion distance of closest approach to the interaction vertex, iii) the cosine of the pointing angle between the D^0-meson candidate line of flight and its reconstructed momentum vector, and iv) the particle identification (PID) information of the decay tracks. The PID information was provided by the specific energy loss and the flight time of particles measured with the TPC and Time Of Flight (TOF) [67] detectors, respectively. Signal samples of prompt and non-prompt D^{*+} mesons for the BDT training were obtained from MC simulations based on the PYTHIA 8.243 event generator [20, 21] with the Monash tune [68] and GEANT 3 package [69] for the propagation of the generated particles through the detector. The background samples were obtained in data from the sideband region of the invariant-mass distribution $\Delta M = M({\rm K}\pi\pi) - M({\rm K}\pi)$. The sideband region was chosen as the invariant-mass interval $\Delta M > 150$ MeV/c^2, where no D^{*+} signal is present. Independent BDTs were trained in three different $p_{\rm T}$ intervals, i.e. $5 < p_{\rm T} < 7$ GeV/c, $7 < p_{\rm T} < 10$ GeV/c, and $10 < p_{\rm T} < 20$ GeV/c. Subsequently, they were applied to the real data sample in which the type of candidate is unknown. The BDT outputs are related to the candidate probability to be a prompt D^{*+} meson, non-prompt D^{*+} meson, or combinatorial background.

The selection based on the probability to be background was optimised to yield a good statistical significance and purity of the signal. By selecting high probability to be prompt or non-prompt D^{*+} mesons, the samples of candidates were further separated to the charm-enhanced (significant contribution of prompt D^{*+} mesons) and the beauty-enhanced (significant contribution of non-prompt D^{*+} mesons) samples. The fractions of prompt ($f_{\rm prompt}$) and non-prompt ($f_{\rm non-prompt}$) D^{*+} mesons in each sample were evaluated with a data-driven method based on the sampling of the raw yield Y_i at different values of the BDT-output score related to the probability of being a non-prompt D^{*+} meson. These fractions can be computed by solving a system of equations that relate raw yields to the corrected yields of prompt ($N_{\rm prompt}$) and non-prompt ($N_{\rm non-prompt}$) D^{*+} mesons by the product of the geometrical acceptance and the detector efficiency factors (Acc $\times\ \varepsilon$) for prompt and non-prompt D^{*+} mesons. Each equation, obtained for a set of selections i, can be expressed as

$$({\rm Acc} \times \varepsilon)_{\rm non-prompt,\it i} \cdot N_{\rm prompt} + ({\rm Acc} \times \varepsilon)_{\rm prompt,\it i} \cdot N_{\rm non-prompt} - Y_i = \delta_{\rm i}, \qquad (2)$$

where $\delta_{\rm i}$ is the residual originating from the uncertainties on Y_i, $({\rm Acc} \times \varepsilon)_{\rm non-prompt,\it i}$, and $({\rm Acc} \times \varepsilon)_{\rm prompt,\it i}$. The system of equation is then solved via a χ^2 minimisation. A detailed description of this method is presented in Refs. [70–72]. For each $p_{\rm T}$ interval, the raw yields of D^{*+} mesons were extracted with a fit to the distribution of the invariant mass ΔM.

The distribution was fitted with a combination of the Gaussian function corresponding to the D^{*+} signal and a background function. The shape of the background distribution can be described with the function $p_0 \sqrt{\Delta M - M_\pi}\ e^{p_1(\Delta M - M_\pi)}$, where p_0 and p_1 are free parameters and M_π is the pion mass. The corresponding Acc $\times\ \varepsilon$ factors were obtained with MC simulations analogous to those used for the BDT trainings. Finally, the fraction of (non-)prompt D^{*+} mesons for a given set of selections was computed
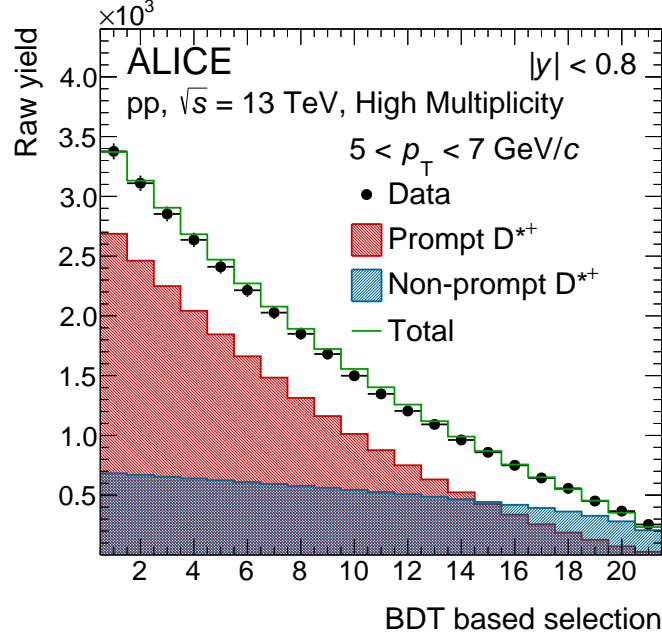
Figure 1: Raw yield as a function of the BDT selection and extracted contributions from prompt and non-prompt D*+ mesons with $5 < p_T < 7$ GeV/c and $|y| < 0.8$ in the high-multiplicity triggered pp collisions at $\sqrt{s} = 13$ TeV.

as

$$f_{\text{(non-)prompt},j} = \frac{(\text{Acc} \times \varepsilon)_{\text{(non-)prompt},j} \cdot N_{\text{(non-)prompt}}}{(\text{Acc} \times \varepsilon)_{\text{prompt},j} \cdot N_{\text{prompt}} + (\text{Acc} \times \varepsilon)_{\text{non-prompt},j} \cdot N_{\text{non-prompt}}}. \tag{3}$$

A different index "j" is used here to underline the fact that not all of these sets are used for the χ^2 minimisation given by Eq. 2. Figure 1 shows an example of a raw-yield extracted as a function of the BDT selection employed in the minimisation procedure for D*+ mesons with $5 < p_T < 7$ GeV/c in high-multiplicity triggered pp collisions at $\sqrt{s} = 13$ TeV. The leftmost data point of the distribution is the raw yield corresponding to the loosest selection on the BDT output related to the candidate probability of being a non-prompt D*+ meson, while the rightmost one corresponds to the strictest selection, which is expected to preferentially select non-prompt D*+ mesons. The prompt and non-prompt components are represented by the red and blue filled histograms, respectively, while their sum is depicted by the green histogram. The f_{prompt} factor obtained in the charm-enhanced sample is higher than 90% for both the high-multiplicity and minimum-bias triggered events, while the $f_{\text{non-prompt}}$ in the beauty-enhanced sample is $\sim 60\%$ and $\sim 40\%$ almost independent of p_T for high-multiplicity and minimum-bias triggered events, respectively.

The raw yields of D*+ mesons were extracted in different $\cos\theta^*$ and p_T intervals for both the beauty- and the charm-enhanced samples. Figure 2 shows the ΔM distributions in $5 < p_T < 7$ GeV/c and $0.0 < \cos\theta^* < 0.2$ intervals for the beauty- and charm-enhanced samples in high-multiplicity triggered pp collisions at $\sqrt{s} = 13$ TeV. The width of the Gaussian function for the D*+ signal was fixed to the value from the MC simulation.

The raw yields were corrected for the corresponding Acc $\times \varepsilon$ factors in each $\cos\theta^*$ and p_T intervals. The impact on the ρ_{00} measurement due to the shape of the $\cos\theta^*$ and p_T distributions in the MC simulations was studied by weighting the generated MC distributions in order to reproduce the measured $\cos\theta^*$ and p_T distributions, and the effect on the Acc $\times \varepsilon$ values was found to be smaller than 0.1% in the analysed p_T intervals. The efficiency and acceptance corrected angular distributions at midrapidity for the selected p_T interval in high-multiplicity triggered pp collisions at $\sqrt{s} = 13$ TeV are shown in Fig. 3. The left panel
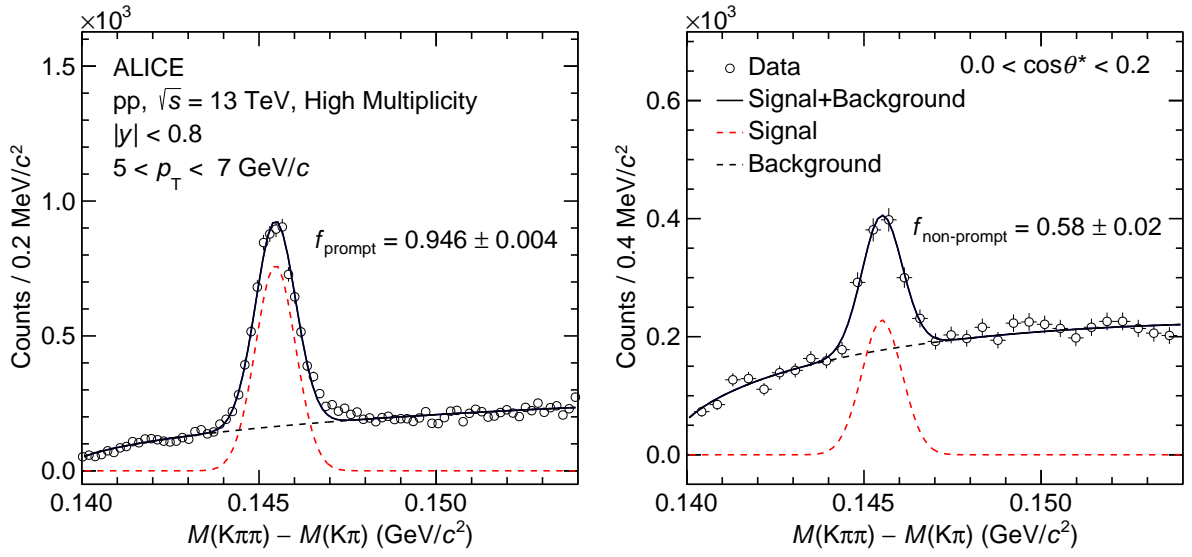
Figure 2: Invariant-mass distributions ΔM for the charm-enhanced (left panel) and the beauty-enhanced (right panel) samples in pp collisions at $\sqrt{s} = 13$ TeV, selected with the high-multiplicity trigger. The distributions are obtained at midrapidity ($|y| < 0.8$) in $5 < p_{\mathrm{T}} < 7$ GeV/c and $0.0 < \cos\theta^* < 0.2$.

of Fig. 3 shows the angular distribution of the beauty-enhanced D^{*+} sample and the right panel shows the same but for the charm-enhanced D^{*+} sample. The absolute value of $\cos\theta^*$ was considered due to
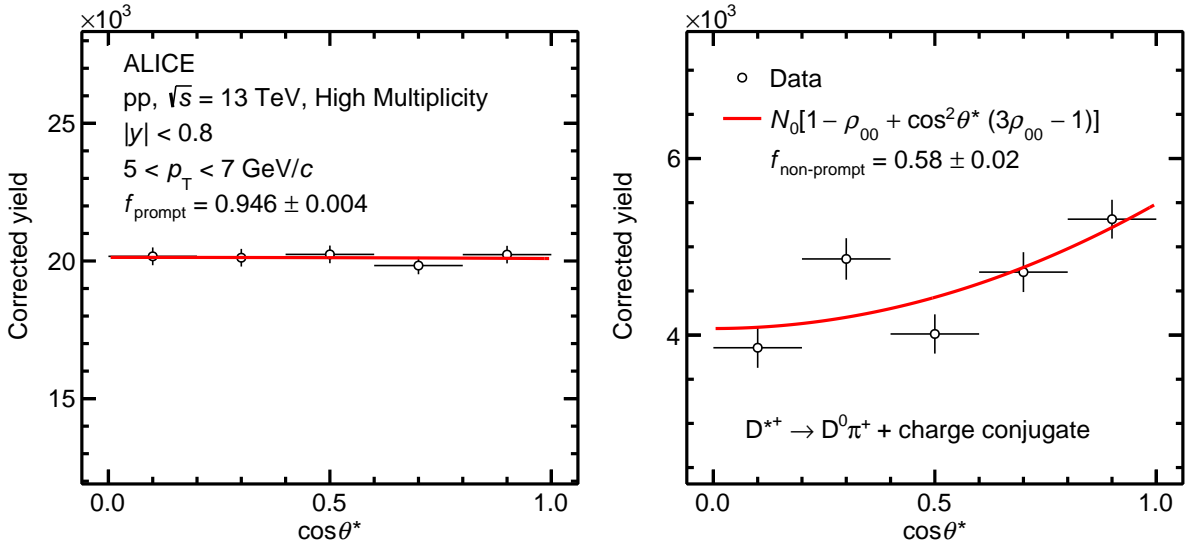

Figure 3: Acceptance and efficiency corrected angular distributions of the decay product in the rest frame of the D^{*+} meson with respect to the helicity axis. The left panel shows the angular distribution for the charm-enhanced D^{*+} sample in pp collisions at $\sqrt{s} = 13$ TeV, selected with the high-multiplicity trigger and the right panel shows the same but for the beauty-enhanced D^{*+} sample. The distributions are obtained at midrapidity ($|y| < 0.8$) in $5 < p_{\mathrm{T}} < 7$ GeV/c and are fitted with Eq. 1 to extract the ρ_{00} values. Only statistical uncertainties are shown.
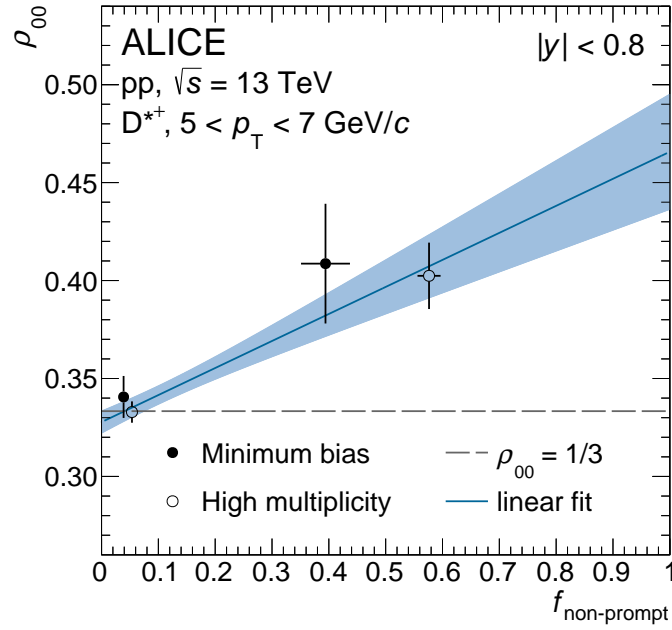
6

Figure 4: The spin density matrix element (ρ_{00}) as a function of $f_{\text{non-prompt}}$ in $5 < p_T < 7$ GeV/c for charm- and beauty-enhanced samples obtained for minimum-bias and high-multiplicity triggered pp collisions at $\sqrt{s} = 13$ TeV. Only statistical uncertainties are shown. The blue line represents the linear fit to the data with the blue band indicating its 1σ confidence interval.

the limited size of the analysed sample. The angular distributions were further fitted with the functional form given in Eq. 1 to extract the ρ_{00} values for both the charm- and the beauty-enhanced samples in each p_T interval.

It was verified with a MC simulation that the ρ_{00} parameter linearly depends on the fraction of non-prompt D^{*+} meson in the analysed sample. Hence, a linear fit of the measured ρ_{00} parameters obtained for the charm- and beauty-enhanced samples as a function of the $f_{\text{non-prompt}}$ was performed to obtain the ρ_{00} values for prompt and non-prompt D^{*+} mesons. The charm- and the beauty-enhanced selections used in this analysis provided two samples of independent candidates. Moreover, the samples of candidates in the minimum-bias and high-multiplicity triggered events are statistically independent. Considering that the measured ρ_{00} parameter can be decomposed as a linear combination of the prompt and non-prompt components,

$$\rho_{00} = f_{\text{prompt}} \cdot \rho_{00}^{\text{prompt}} + f_{\text{non-prompt}} \cdot \rho_{00}^{\text{non-prompt}}, \tag{4}$$

the four independent measurements corresponding to the charm- and beauty-enhanced samples for both minimum-bias and high-multiplicity events were fitted with a linear function in order to extrapolate it to $f_{\text{non-prompt}} = 0$ and $f_{\text{non-prompt}} = 1$. A similar procedure was adopted in Ref. [73] to measure the elliptic flow of prompt and non-prompt D mesons. With the current data samples it is not possible to perform the linear extrapolation of the ρ_{00} parameter independently for the minimum-bias and high-multiplicity collisions, which may have different physical origin, and the reported results are for the combined sample. Figure 4 shows the linear fit of ρ_{00} as a function of $f_{\text{non-prompt}}$ in $5 < p_T < 7$ GeV/c. The filled (empty) markers correspond to the measurements performed in the minimum-bias (high-multiplicity) pp collisions. The coloured band represents the 1σ confidence interval obtained from the linear fit. The ρ_{00} parameter for prompt and non-prompt D^{*+} mesons is then obtained by evaluating the fit function for $f_{\text{non-prompt}} = 0$ and $f_{\text{non-prompt}} = 1$, respectively.

Table 1: Summary of the relative systematic uncertainties on the ρ_{00} parameter of prompt and non-prompt D*+ mesons for different p_T intervals.

	Prompt		Non-prompt	
p_T (GeV/c)	5–7	10–20	5–7	10–20
Signal yield	2.0%	0.5%	4.0%	2.0%
Tracking efficiency	negl.	1.0%	2.0%	4.0%
BDT efficiency	0.5%	3.5%	6.0%	5.0%
(Non-)prompt fraction	negl.	negl.	0.5%	negl.
Total	2.5%	3.5%	8.0%	6.5%

3 Systematic uncertainties

There are four major sources of systematic uncertainties in the measurement of ρ_{00} for prompt and non-prompt D*+ mesons. These uncertainties are related to: i) the signal extraction, ii) the track reconstruction and selection efficiencies, iii) the BDT selection efficiency, and iv) the (non-)prompt fraction estimation. The systematic uncertainty arising from the signal extraction was estimated by varying the invariant-mass fit range, leaving the Gaussian width free in the fit, and using a bin-counting method for the raw-yield extraction. In the bin-counting method the signal yield is extracted by integrating the invariant-mass distribution after subtracting the background estimated from the background fit function. The systematic uncertainty associated with the track selection and reconstruction efficiency was evaluated by varying the track-quality selection criteria as described in Ref. [74]. The systematic uncertainty on the selection efficiency originates from imperfections in the description of the decay kinematics as well as the detector resolution and alignment in the simulation. It was estimated by comparing the ρ_{00} parameters obtained for prompt and non-prompt D*+ mesons with different BDT selection criteria. The uncertainty associated with the (non-)prompt fraction estimation was evaluated by varying the selection criteria described in Sec. 2, as well as the configuration of the invariant-mass fits. All of the above mentioned variations were performed independently and, assuming they are uncorrelated with each other, added in quadrature to obtain the total systematic uncertainties. Table 1 summarises the values of the systematic uncertainties for the lowest and highest p_T intervals, reporting separately the various sources for prompt and non-prompt D*+ mesons. The total systematic uncertainty ranges between 2.5% and 3.5% for prompt D*+ mesons, and between 6.5% and 8% for non-prompt D*+ mesons.

In order to validate the results of the measurements, an additional analysis was performed with respect to a random quantisation axis (random unit vector direction in 3-dimensional space) which breaks the correlation between the helicity axis and the daughter momentum direction, due to helicity conservation. As expected, the extracted ρ_{00} values for both prompt and non-prompt D*+ mesons are consistent with 1/3.

4 Results

Figure 5 shows the ρ_{00} values with respect to the helicity axis for prompt and non-prompt D*+ mesons as a function of p_T in pp collisions at $\sqrt{s} = 13$ TeV. The measurements are performed in $|y| < 0.8$. The ρ_{00} values for prompt D*+ mesons are consistent with 1/3, while for non-prompt D*+ mesons they are significantly larger than 1/3 throughout the studied p_T range. The values measured in the three p_T intervals were averaged using the corrected yields of prompt and non-prompt D*+ mesons as weights.
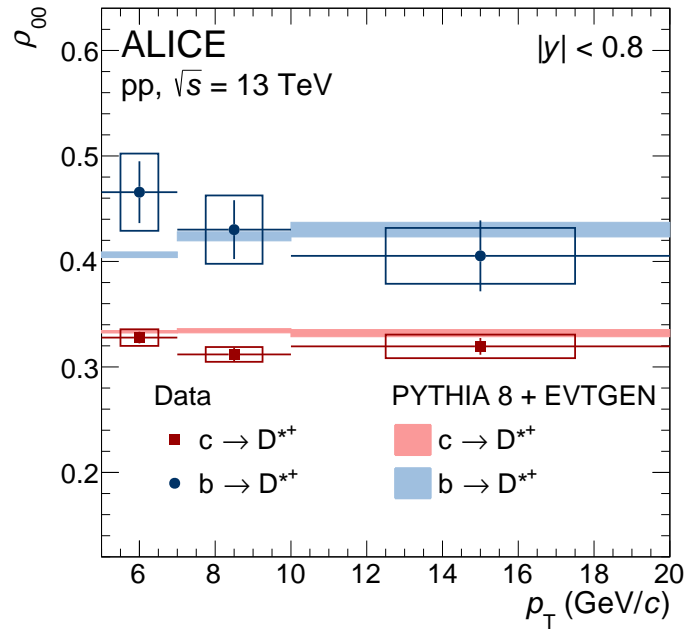
Figure 5: The spin density matrix element (ρ_{00}) for prompt and non-prompt D*+ mesons as a function of p_{T} in pp collisions at $\sqrt{s} = 13$ TeV. Measurements are carried out with respect to the helicity axis at $|y| < 0.8$. Statistical and systematic uncertainties are represented by bars and boxes, respectively. The measurements are compared with the estimations from the QCD-based MC event generator PYTHIA 8 + EVTGEN [68, 75]. Model estimations are shown by colour bands where the width of the band corresponds to the statistical uncertainty in model calculations.

The resulting ρ_{00} values in the p_{T} interval between 5 and 20 GeV/c are

$$\rho_{00}(\text{prompt D}^{*+}) = 0.324 \pm 0.004(\text{stat.}) \pm 0.008(\text{syst.}),$$
$$\rho_{00}(\text{non-prompt D}^{*+}) = 0.455 \pm 0.022(\text{stat.}) \pm 0.035(\text{syst.}). \tag{5}$$

This finding implies no spin alignment for prompt D*+ mesons with a simultaneous non-zero spin alignment of non-prompt D*+ mesons in high-energy pp collisions. The evidence of non-prompt D*+-meson spin alignment can be understood as a consequence of helicity conservation in the decay of beauty scalar mesons to vector mesons. Measured ρ_{00} values are further compared with the MC event generator PYTHIA 8 + EVTGEN [68, 75]. The EVTGEN decay package, which conserves the helicity and account for the V−A nature in the decay of beauty mesons, is used in place of the default PYTHIA 8 decayer. In this case, model calculations are found to be in agreement with the extracted ρ_{00} values for both prompt and non-prompt D*+ mesons, while if the EVTGEN package is not used, the ρ_{00} parameter is found to be compatible with 1/3 for both prompt and non-prompt D*+ mesons. The measured ρ_{00} for non-prompt D*+ mesons is qualitatively consistent with the longitudinal polarisation fraction (f_{L}) observed by the LHCb collaboration in the $\mathrm{B}^0 \to \mathrm{D}^{*-}\mathrm{D}_{\mathrm{s}}^{*+}$ decay with respect to a different quantisation axis defined by the B-meson momentum direction [53]. The direct comparison between the magnitudes of f_{L} and ρ_{00} measured by the LHCb and ALICE Collaborations is not possible due to the different quantisation axis and the different decay channels. Therefore, dedicated model calculations are required for a quantitative comparison of the ALICE and LHCb data.

The presented results for pp collisions can be used to estimate the magnitude of the corresponding contribution to the spin alignment in heavy-ion collisions. In particular, the spin alignment of non-prompt D*+ meson with respect to the helicity axis can affect the measurements of D*+ spin alignment with respect to the reaction plane in heavy-ion collisions. Due to the elliptic flow of the non-prompt D*+

mesons [49, 50, 76–78] in heavy-ion collisions, the helicity axis is correlated to the direction of the angular momentum and the magnetic field, which are perpendicular to the orientation of the reaction plane [49]. In order to obtain a quantitative estimate of this effect for heavy-ion collisions, a combination of PYTHIA 8 and the EVTGEN decay package, which are in good agreement with ALICE measurements as shown in Fig. 5, is used to model the spin alignment of non-prompt D^{*+}-mesons with respect to the helicity axis. Elliptic flow modulations of non-prompt D^{*+} mesons are introduced in the simulation by an appropriate rotation of the D^{*+} and its decay product momentum in the azimuthal plane. Introducing v_2 modulation aligns the momentum direction of non-prompt D^{*+} in the direction perpendicular to the reaction plane. Two different calculations with v_2 values of 0.05 and 0.1 were performed. These values were chosen to mimic measurements reported by the ALICE and ATLAS Collaborations of leptons from beauty-hadron decays for midcentral Pb–Pb collisions [79, 80]. Figure 6 shows the calculated ρ_{00} values for D^{*+} mesons as a function of $f_{\text{non-prompt}}$ with respect to the direction perpendicular to the reaction plane. It is found that in the presence of v_2, helicity conservation in the beauty-meson decay leads to a value of ρ_{00} less than $1/3$. The opposite direction with respect to $1/3$ compared to the measurement presented in this letter is due to the different quantisation axis. In the recombination hadronisation scenario of polarised quarks, the expected value of ρ_{00} for both the magnetic field and angular momentum is also less than $1/3$ [41]. Therefore, in the presence of v_2 the spin alignment of non-prompt D^{*+} mesons due to the helicity conservation in beauty-meson decays mimics the signal of global spin alignment, expected due to the presence of large angular momentum and magnetic field in midcentral heavy-ion collisions. In the presence of additional non-flow correlations (i.e. correlations not induced by the collective expansion but rather by decays and jet contributions) [81], this effect can get further enhanced. A sizeable fraction of non-prompt D^{*+} mesons, e.g. $f_{\text{non-prompt}} = 0.2$ [70, 72] can give on the order of 5% deviation from the $\rho_{00} = 1/3$. This contribution is not negligible considering the recent J/ψ polarisation measurement in Pb–Pb collisions by the ALICE Collaboration where a deviation up to 10% from the $\rho_{00} = 1/3$ was observed [51]. Future measurements with non-prompt charm hadrons of the spin alignment in pp collisions and azimuthal anisotropy in heavy-ion collisions will provide a solid baseline for understanding effects induced by the initial angular momentum and magnetic field in non-central heavy-ion collisions.

5   Summary

The first measurements for prompt and non-prompt D^{*+} meson spin alignment with respect to the helicity axis at midrapidity in pp collisions at $\sqrt{s} = 13$ TeV are presented. No spin alignment is observed for the prompt D^{*+} mesons in pp collisions, with measured ρ_{00} values being consistent with $1/3$. This observation is consistent with previous measurements in e$^+$e$^-$ collisions far from the Z^0 resonance and suggests that charm quarks are either produced unpolarised or their polarisation is washed out during the hadronisation process. The measured value for the non-prompt D^{*+}-meson spin density element is $\rho_{00} = 0.455 \pm 0.022(\text{stat.}) \pm 0.035(\text{syst.})$ in the $5 < p_T < 20$ GeV/c interval. The measured value is compatible with the prediction from PYTHIA 8 + EVTGEN simulations and is interpreted as an evidence of spin alignment of non-prompt D^{*+} mesons with respect to the helicity axis due to the helicity conservation in beauty-meson decays. Based on the measurements and MC simulations, it was estimated that the spin alignment of the non-prompt D^{*+} mesons in the presence of elliptic flow can mimic the signal of global spin alignment in heavy-ion collisions. The new data presented in this letter provide an important baseline for future spin alignment measurements of D^{*+} vector mesons in heavy-ion collisions, which probe the initial angular momentum and magnetic field.

References

[1] L. Gladilin, "Fragmentation fractions of c and b quarks into charmed hadrons at LEP", *Eur. Phys. J. C* **75** (2015) 19, arXiv:1404.3888 [hep-ex].
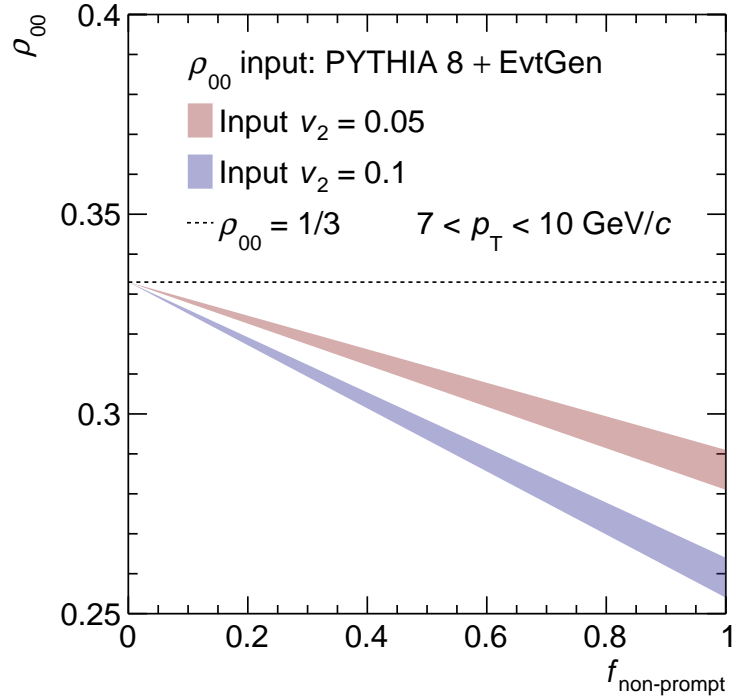
Figure 6: Model simulation based on the MC event generator PYTHIA 8 + EVTGEN [68, 75] for the spin density matrix element (ρ_{00}) for D^{*+} mesons with respect to the direction perpendicular to the reaction plane as a function of $f_{\text{non-prompt}}$. Model simulations are carried out for D^{*+} mesons at midrapidity ($|y| < 0.8$) with two input values of v_2.

[2] **ALICE** Collaboration, S. Acharya *et al.*, "Charm-quark fragmentation fractions and production cross section at midrapidity in pp collisions at the LHC", *Phys. Rev. D* **105** (2022) L011103, arXiv:2105.06335 [nucl-ex].

[3] **LHCb** Collaboration, R. Aaij *et al.*, "Measurement of B hadron fractions in 13 TeV pp collisions", *Phys. Rev. D* **100** (2019) 031102, arXiv:1902.06794 [hep-ex].

[4] **HFLAV** Collaboration, Y. S. Amhis *et al.*, "Averages of b-hadron, c-hadron, and τ-lepton properties as of 2018", *Eur. Phys. J. C* **81** (2021) 226, arXiv:1909.12524 [hep-ex].

[5] **ALICE** Collaboration, S. Acharya *et al.*, "Observation of a multiplicity dependence in the p_{T}-differential charm baryon-to-meson ratios in proton-proton collisions at $\sqrt{s} = 13$ TeV", *Phys. Lett. B* **829** (2022) 137065, arXiv:2111.11948 [nucl-ex].

[6] **ALICE** Collaboration, "First measurement of Ω_{c}^0 production in pp collisions at $\sqrt{s} = 13$ TeV", arXiv:2205.13993 [nucl-ex].

[7] **LHCb** Collaboration, "Evidence for modification of b quark hadronization in high-multiplicity pp collisions at $\sqrt{s} = 13$ TeV", arXiv:2204.13042 [hep-ex].

[8] **LHCb** Collaboration, R. Aaij *et al.*, "Precise measurement of the $f_{\text{s}}/f_{\text{d}}$ ratio of fragmentation fractions and of B$_{\text{s}}^0$ decay branching fractions", *Phys. Rev. D* **104** (2021) 032005, arXiv:2103.06810 [hep-ex].

[9] A. F. Falk and M. E. Peskin, "Production, decay, and polarization of excited heavy hadrons", *Phys. Rev. D* **49** (1994) 3320–3332, arXiv:hep-ph/9308241.

[10] J. G. Korner, A. Pilaftsis, and M. M. Tung, "One Loop QCD Mass effects in the production of polarized bottom and top quarks", *Z. Phys. C* **63** (1994) 575–579, `arXiv:hep-ph/9311332`.

[11] T. Mannel and G. A. Schuler, "Semileptonic decays of bottom baryons at LEP", *Phys. Lett. B* **279** (1992) 194–200.

[12] **ALEPH** Collaboration, D. Buskulic *et al.*, "Measurement of Λ_b polarization in Z decays", *Phys. Lett. B* **365** (1996) 437–447.

[13] **DELPHI** Collaboration, P. Abreu *et al.*, "Λ_b polarization in Z^0 decays at LEP", *Phys. Lett. B* **474** (2000) 205–222.

[14] **OPAL** Collaboration, G. Abbiendi *et al.*, "Measurement of the average polarization of b baryons in hadronic Z^0 decays", *Phys. Lett. B* **444** (1998) 539–554, `arXiv:hep-ex/9808006`.

[15] **LHCb** Collaboration, R. Aaij *et al.*, "Measurements of the $\Lambda_b^0 \to J/\psi\Lambda$ decay amplitudes and the Λ_b^0 polarisation in pp collisions at $\sqrt{s} = 7$ TeV", *Phys. Lett. B* **724** (2013) 27–35, `arXiv:1302.5578 [hep-ex]`.

[16] J. F. Donoghue, "Comment on polarized fragmentation functions", *Phys. Rev. D* **19** (1979) 2806.

[17] I. I. Bigi, "Some quantitative estimates about final-state polarization in deep inelastic lepton-nucleon scattering", *Nuov. Cim. A* **41** (1977) 581–591.

[18] J. E. Augustin and F. M. Renard, "How to Measure Quark Helicities in e + e− → Hadrons", ECFA-LEP-49. `https://cds.cern.ch/record/867018`.

[19] B. Andersson, G. Gustafson, G. Ingelman, and T. Sjostrand, "Parton Fragmentation and String Dynamics", *Phys. Rept.* **97** (1983) 31–145.

[20] T. Sjostrand, S. Mrenna, and P. Z. Skands, "PYTHIA 6.4 Physics and Manual", *JHEP* **05** (2006) 026, `arXiv:hep-ph/0603175`.

[21] T. Sjöstrand *et al.*, "An introduction to PYTHIA 8.2", *Comput. Phys. Commun.* **191** (2015) 159–177, `arXiv:1410.3012 [hep-ph]`.

[22] B. P. Kersevan and E. Richter-Was, "The Monte Carlo event generator AcerMC versions 2.0 to 3.8 with interfaces to PYTHIA 6.4, HERWIG 6.5 and ARIADNE 4.1", *Comput. Phys. Commun.* **184** (2013) 919–985, `arXiv:hep-ph/0405247`.

[23] J. Bellm *et al.*, "Herwig 7.0/Herwig++ 3.0 release note", *Eur. Phys. J. C* **76** (2016) 196, `arXiv:1512.01178 [hep-ph]`.

[24] **DELPHI** Collaboration, P. Abreu *et al.*, "B* production in Z decays", *Z. Phys. C* **68** (1995) 353–362.

[25] **ALEPH** Collaboration, D. Buskulic *et al.*, "Production of excited beauty states in Z decays", *Z. Phys. C* **69** (1996) 393–404.

[26] **OPAL** Collaboration, K. Ackerstaff *et al.*, "Study of $\phi(1020)$, D$^{*\pm}$ and B* spin alignment in hadronic Z^0 decays", *Z. Phys. C* **74** (1997) 437–449.

[27] **TPC/Two-Gamma** Collaboration, H. Aihara *et al.*, "Test of spin dependence in charm-quark fragmentation to D*", *Phys. Rev. D* **43** (1991) 29–33.

[28] **HRS** Collaboration, S. Abachi *et al.*, "Measurement of the Spin Density Matrix of D* Mesons Produced in e$^+$e$^-$ Annihilations", *Phys. Lett. B* **199** (1987) 585–590.

[29] **CLEO** Collaboration, Y. Kubota *et al.*, "Study of continuum D^{*+} spin alignment", *Phys. Rev. D* **44** (1991) 593–600.

[30] F. Becattini, F. Piccinini, and J. Rizzo, "Angular momentum conservation in heavy ion collisions at very high energy", *Phys. Rev.* **C77** (2008) 024906, `arXiv:0711.1253 [nucl-th]`.

[31] D. E. Kharzeev, L. D. McLerran, and H. J. Warringa, "The Effects of topological charge change in heavy ion collisions: 'Event by event P and CP violation'", *Nucl. Phys.* **A803** (2008) 227–253, `arXiv:0711.0950 [hep-ph]`.

[32] V. Skokov, A. Y. Illarionov, and V. Toneev, "Estimate of the magnetic field strength in heavy-ion collisions", *Int. J. Mod. Phys. A* **24** (2009) 5925–5932, `arXiv:0907.1396 [nucl-th]`.

[33] W.-T. Deng and X.-G. Huang, "Event-by-event generation of electromagnetic fields in heavy-ion collisions", *Phys. Rev. C* **85** (2012) 044907, `arXiv:1201.5108 [nucl-th]`.

[34] P. Braun-Munzinger, V. Koch, T. Schäfer, and J. Stachel, "Properties of hot and dense matter from relativistic heavy ion collisions", *Phys. Rept.* **621** (2016) 76–126, `arXiv:1510.00442 [nucl-th]`.

[35] Z.-T. Liang and X.-N. Wang, "Globally polarized quark-gluon plasma in non-central A+A collisions", *Phys. Rev. Lett.* **94** (2005) 102301, `arXiv:nucl-th/0410079 [nucl-th]`. [Erratum: *Phys. Rev. Lett.* **96** (2006) 039901].

[36] P. Christakoglou, S. Qiu, and J. Staa, "Systematic study of the chiral magnetic effect with the AVFD model at LHC energies", *Eur. Phys. J. C* **81** (2021) 717, `arXiv:2106.03537 [nucl-th]`.

[37] E. S. Fraga and A. J. Mizher, "Chiral transition in a strong magnetic background", *Phys. Rev. D* **78** (2008) 025016, `arXiv:0804.1452 [hep-ph]`.

[38] A. Andronic *et al.*, "Heavy-flavour and quarkonium production in the LHC era: from proton–proton to heavy-ion collisions", *Eur. Phys. J. C* **76** (2016) 107, `arXiv:1506.03981 [nucl-ex]`.

[39] Z.-T. Liang and X.-N. Wang, "Spin alignment of vector mesons in non-central A+A collisions", *Phys. Lett.* **B629** (2005) 20–26, `arXiv:nucl-th/0411101 [nucl-th]`.

[40] Z.-T. Liang, "Global polarization of QGP in non-central heavy ion collisions at high energies", *J. Phys.* **G34** (2007) S323–330, `arXiv:0705.2852 [nucl-th]`.

[41] Y.-G. Yang, R.-H. Fang, Q. Wang, and X.-N. Wang, "Quark coalescence model for polarized vector mesons and baryons", *Phys. Rev.* **C97** (2018) 034917, `arXiv:1711.06008 [nucl-th]`.

[42] **ALICE** Collaboration, S. Acharya *et al.*, "Prompt D^0, D$^+$, and D^{*+} production in Pb–Pb collisions at $\sqrt{s_{NN}} = 5.02$ TeV", *JHEP* **01** (2022) 174, `arXiv:2110.09420 [nucl-ex]`.

[43] **CMS** Collaboration, A. M. Sirunyan *et al.*, "Nuclear modification factor of D^0 mesons in PbPb collisions at $\sqrt{s_{NN}} = 5.02$ TeV", *Phys. Lett. B* **782** (2018) 474–496, `arXiv:1708.04962 [nucl-ex]`.

[44] **ALICE** Collaboration, S. Acharya *et al.*, "Measurement of prompt D$_s^+$-meson production and azimuthal anisotropy in Pb–Pb collisions at $\sqrt{s_{NN}}=5.02$TeV", *Phys. Lett. B* **827** (2022) 136986, `arXiv:2110.10006 [nucl-ex]`.

[45] **STAR** Collaboration, J. Adam *et al.*, "Observation of D$_s^\pm$/D^0 enhancement in Au+Au collisions at $\sqrt{s_{NN}} = 200$ GeV", *Phys. Rev. Lett.* **127** (2021) 092301, `arXiv:2101.11793 [hep-ex]`.

[46] **ALICE** Collaboration, S. Acharya *et al.*, "Constraining hadronization mechanisms with Λ_c^+/D^0 production ratios in Pb–Pb collisions at $\sqrt{s_{NN}} = 5.02$ TeV", `arXiv:2112.08156 [nucl-ex]`.

[47] **CMS** Collaboration, A. M. Sirunyan *et al.*, "Production of Λ_c^+ baryons in proton-proton and lead-lead collisions at $\sqrt{s_{NN}} = 5.02$ TeV", *Phys. Lett. B* **803** (2020) 135328, `arXiv:1906.03322 [hep-ex]`.

[48] **STAR** Collaboration, J. Adam *et al.*, "First measurement of Λ_c baryon production in Au+Au collisions at $\sqrt{s_{NN}} = 200$ GeV", *Phys. Rev. Lett.* **124** (2020) 172301, `arXiv:1910.14628 [nucl-ex]`.

[49] **ALICE** Collaboration, S. Acharya *et al.*, "Transverse-momentum and event-shape dependence of D-meson flow harmonics in Pb–Pb collisions at $\sqrt{s_{NN}} = 5.02$ TeV", *Phys. Lett. B* **813** (2021) 136054, `arXiv:2005.11131 [nucl-ex]`.

[50] **CMS** Collaboration, A. M. Sirunyan *et al.*, "Measurement of prompt D^0 and $\overline{D}^0$ meson azimuthal anisotropy and search for strong electric fields in PbPb collisions at $\sqrt{s_{NN}} = 5.02$ TeV", *Phys. Lett. B* **816** (2021) 136253, `arXiv:2009.12628 [hep-ex]`.

[51] **ALICE** Collaboration, "Measurement of the J/ψ polarization with respect to the event plane in Pb–Pb collisions at the LHC", `arXiv:2204.10171 [nucl-ex]`.

[52] **Belle** Collaboration, A. Abdesselam *et al.*, "Measurement of the D^{*-} polarization in the decay $B^0 \to D^{*-}\tau^+\nu_\tau$",. `arXiv:1903.03102 [hep-ex]`.

[53] **LHCb** Collaboration, R. Aaij *et al.*, "Angular analysis of $B^0 \to D^{*-}D_s^{*+}$ with $D_s^{*+} \to D_s^+\gamma$ decays", *JHEP* **06** (2021) 177, `arXiv:2105.02596 [hep-ex]`.

[54] M. Suzuki, "Final-state interactions and s^- quark helicity conservation in $B \to J/\psi K^*$", *Phys. Rev. D* **64** (2001) 117503, `arXiv:hep-ph/0106354`.

[55] **BaBar** Collaboration, B. Aubert *et al.*, "Time-Dependent and Time-Integrated Angular Analysis of B -> phi Ks pi0 and B -> phi K+ pi-", *Phys. Rev. D* **78** (2008) 092008, `arXiv:0808.3586 [hep-ex]`.

[56] U. Fano, "Description of States in Quantum Mechanics by Density Matrix and Operator Techniques", *Rev. Mod. Phys.* **29** (1957) 74–93.

[57] R. Snellings, "Elliptic Flow: A Brief Review", *New J. Phys.* **13** (2011) 055008, `arXiv:1102.3010 [nucl-ex]`.

[58] K. Schilling, P. Seyboth, and G. E. Wolf, "On the Analysis of Vector Meson Production by Polarized Photons", *Nucl. Phys.* **B15** (1970) 397–412. [Erratum: *Nucl. Phys. B* **18** (1970) 332].

[59] **ALICE** Collaboration, B. B. Abelev *et al.*, "Performance of the ALICE Experiment at the CERN LHC", *Int. J. Mod. Phys. A* **29** (2014) 1430044, `arXiv:1402.4476 [nucl-ex]`.

[60] **ALICE** Collaboration, K. Aamodt *et al.*, "The ALICE experiment at the CERN LHC", *JINST* **3** (2008) S08002.

[61] **ALICE** Collaboration, E. Abbas *et al.*, "Performance of the ALICE VZERO system", *JINST* **8** (2013) P10016, `arXiv:1306.3130 [nucl-ex]`.

[62] **ALICE** Collaboration, K. Aamodt *et al.*, "Alignment of the ALICE Inner Tracking System with cosmic-ray tracks", *JINST* **5** (2010) P03003, `arXiv:1001.0502 [physics.ins-det]`.

[63] **Particle Data Group** Collaboration, R. L. Workman *et al.*, "Review of Particle Physics", *PTEP* **2022** (2022) 083C01.

[64] J. Alme *et al.*, "The ALICE TPC, a large 3-dimensional tracking device with fast readout for ultra-high multiplicity events", *Nucl. Instrum. Meth. A* **622** (2010) 316–367, `arXiv:1001.1950` `[physics.ins-det]`.

[65] T. Chen and C. Guestrin, "Xgboost: A scalable tree boosting system", *Proceedings of the 22nd ACM SIGKDD International Conference on Knowledge Discovery and Data Mining* (2016) 785–794, `arXiv:1603.02754` `[cs.LG]`.

[66] L. Barioglio, F. Catalano, M. Concas, P. Fecchio, F. Grosa, F. Mazzaschi, and M. Puccio, "hipe4ml/hipe4ml", July, 2021. `https://doi.org/10.5281/zenodo.5070132`.

[67] A. Akindinov *et al.*, "Performance of the ALICE Time-Of-Flight detector at the LHC", *Eur. Phys. J. Plus* **128** (2013) 44.

[68] P. Skands, S. Carrazza, and J. Rojo, "Tuning PYTHIA 8.1: the Monash 2013 Tune", *Eur. Phys. J. C* **74** (2014) 3024, `arXiv:1404.5630` `[hep-ph]`.

[69] R. Brun, F. Bruyant, F. Carminati, S. Giani, M. Maire, A. McPherson, G. Patrick, and L. Urban, *GEANT: Detector Description and Simulation Tool; Oct 1994.* CERN Program Library. CERN, Geneva, 1993. `http://cds.cern.ch/record/1082634`. Long Writeup W5013.

[70] **ALICE** Collaboration, S. Acharya *et al.*, "Measurement of beauty and charm production in pp collisions at $\sqrt{s} = 5.02$ TeV via non-prompt and prompt D mesons", *JHEP* **05** (2021) 220, `arXiv:2102.13601` `[nucl-ex]`.

[71] **ALICE** Collaboration, S. Acharya *et al.*, "First study of the two-body scattering involving charm hadrons", *Phys. Rev. D* **106** (2022) 052010, `arXiv:2201.05352` `[nucl-ex]`.

[72] **ALICE** Collaboration, S. Acharya *et al.*, "Measurement of beauty production via non-prompt D^0 mesons in Pb–Pb collisions at $\sqrt{s_{NN}} = 5.02$ TeV", `arXiv:2202.00815` `[nucl-ex]`.

[73] **CMS** Collaboration, A. M. Sirunyan *et al.*, "Studies of charm and beauty hadron long-range correlations in pp and pPb collisions at LHC energies", *Phys. Lett. B* **813** (2021) 136036, `arXiv:2009.07065` `[hep-ex]`.

[74] **ALICE** Collaboration, S. Acharya *et al.*, "Measurement of D-meson production at mid-rapidity in pp collisions at $\sqrt{s} = 7$ TeV", *Eur. Phys. J. C* **77** (2017) 550, `arXiv:1702.00766` `[hep-ex]`.

[75] D. J. Lange, "The EvtGen particle decay simulation package", *Nucl. Instrum. Meth. A* **462** (2001) 152–155.

[76] **ALICE** Collaboration, S. Acharya *et al.*, "D-meson azimuthal anisotropy in midcentral Pb–Pb collisions at $\sqrt{s_{NN}} = 5.02$ TeV", *Phys. Rev. Lett.* **120** (2018) 102301, `arXiv:1707.01005` `[nucl-ex]`.

[77] **CMS** Collaboration, A. M. Sirunyan *et al.*, "Measurement of prompt D^0 meson azimuthal anisotropy in Pb–Pb collisions at $\sqrt{s_{NN}} = 5.02$ TeV", *Phys. Rev. Lett.* **120** (2018) 202301, `arXiv:1708.03497` `[nucl-ex]`.

[78] **ALICE** Collaboration, S. Acharya *et al.*, "Event-shape engineering for the D-meson elliptic flow in mid-central Pb–Pb collisions at $\sqrt{s_{NN}} = 5.02$ TeV", *JHEP* **02** (2019) 150, `arXiv:1809.09371` `[nucl-ex]`.

[79] **ALICE** Collaboration, S. Acharya *et al.*, "Elliptic Flow of Electrons from Beauty-Hadron Decays in Pb–Pb Collisions at $\sqrt{s_{\mathrm{NN}}} = 5.02$ TeV", *Phys. Rev. Lett.* **126** (2021) 162001, arXiv:2005.11130 [nucl-ex].

[80] **ATLAS** Collaboration, G. Aad *et al.*, "Measurement of azimuthal anisotropy of muons from charm and bottom hadrons in Pb–Pb collisions at $\sqrt{s_{\mathrm{NN}}} = 5.02$ TeV with the ATLAS detector", *Phys. Lett. B* **807** (2020) 135595, arXiv:2003.03565 [nucl-ex].

[81] N. Borghini, P. M. Dinh, and J.-Y. Ollitrault, "Are flow measurements at SPS reliable?", *Phys. Rev. C* **62** (2000) 034902, arXiv:nucl-th/0004026.